Available online at www.sciencedirect.com

SciVerse ScienceDirect

Ceramics International 39 (2013) 3779–3787

CERAMICS INTERNATIONAL

www.elsevier.com/locate/ceramint

Synthesis and photocatalysis of TiO_2 hollow spheres by a facile template-implantation route

Wenjea J. Tseng*, Po-Sung Chao

Department of Materials Science and Engineering, National Chung Hsing University, 250 Kuo Kuang Road, Taichung 402, Taiwan

Received 8 August 2012; received in revised form 14 October 2012; accepted 17 October 2012
Available online 24 October 2012

Abstract

Process variables such as reaction temperature (55 to 90 °C), calcination temperature (450 to 750 °C), and concentration of $TiCl_4$ precursor (26 to 105 mM) have been examined in order to tailor the surface area, crystallite size, and the anatase/rutile ratio of the polycrystalline TiO_2 microcapsules prepared by a template-implantation route in heptane solvent. The hollow capsules are all non-aggregating with nanoporous shell structure. Among the process variables examined, the Brunauer–Emmett–Teller (BET) surface area and the anatase/rutile ratio are found critically dependent on the reaction temperature, in which a reduced reaction temperature (from 90 to 55 °C) leads to a higher BET value (from 8.4 to 36.4 $m^{-2}\,g^{-1}$), a predominant anatase phase (weight fraction of the anatase phase increases from 0.20 to 0.84), and an improved photodegradation of aqueous methylene blue (MB) dye under UV exposure (the degradation rate increases from 0.5×10^{-2} to $5.5\times10^{-2}\,min^{-1}$).

Keywords: A.Implantation; TiO_2 capsule; Template; Photocatalysis

1. Introduction

Titanium dioxide (TiO_2) in both powdered and thin-film forms is of great importance from energy and environment viewpoints owing mainly to its promising use in cost-effective photovoltaic and photocatalytic devices [1–5]. Mesoporous TiO_2 hollow spheres with tunable shell and cavity, in particular, have shown an enhanced photocatalytic activity under UV irradiation [6–10]. In view of the literature, many methods have been developed to prepare the TiO_2 hollow spheres. Caruso et al. [11] were the first to employ an electrostatic layer-by-layer (LBL) deposition of inorganic TiO_2 precursors in alternation with oppositely charged polyelectrolyte to form multilayer coating on colloidal templates. TiO_2 hollow spheres with a well-defined particle size, size distribution, and shell thickness were obtained by subsequent removal of the template core through calcination or solvent dissolution. Similarly, Wang et al. [12] prepared TiO_2 hollow spheres by a sequential LBL assembly using exfoliated TiO_2 nanosheets as the shell's building block together with polyethylenimine as the surface-charge modifier for the polymeric template beads. A precise control on the shell thickness was obtained by the nanosheets used. In addition to the electrostatic adsorption, Chen et al. [13] encapsulated TiO_2 nanoparticles in reverse micelles before the shell deposition takes place. This produces a hydrophilic/hydrophobic interaction in addition to the electrostatic effect to facilitate the shell formation in a suitable hydrophobic solvent, and extends the LBL process to a wider spectrum of core–shell pairs in materials selection. TiO_2 capsules have also been prepared by a direct chemical deposition in which a rapidly hydrolyzed coating of negatively charged TiO_2 precipitates deposits preferentially on positively charged colloidal templates [14,15]. Imhof [14] demonstrated that the coating thickness can be easily tuned through a seeded growth method. Apart from the use of discrete hard template, TiO_2 hollows spheres were also synthesized from templating against arrays of colloidal crystals [16], use of soft templates (e.g., emulsion droplets, micelles, vesicles, etc.) [17–21], and template-free approaches as well [9,22,23].

The hard-templating approach is still considered by many the most reliable and robust method to date in

*Corresponding author. Tel.: +886 4 2287 0720; fax: +886 4 2285 7017.
E-mail address: wenjea@dragon.nchu.edu.tw (W.J. Tseng).

0272-8842/$ - see front matter © 2012 Elsevier Ltd and Techna Group S.r.l. All rights reserved.
http://dx.doi.org/10.1016/j.ceramint.2012.10.217

fabricating hollow particles with a well-defined shape, size, and particle-size distribution in relatively large quantities [23]. In our previous works, non-aggregating hollow spheres of different compositions (e.g., Al_2O_3 [24], In_2O_3 [25,26], Al_2O_3/Pt [26], and Er-doped TiO_2 [27]) have been prepared by a facile synthesis route involving use of commercial polymeric beads consisting of resin grafted polydivinylbenzene (PDVB) as the sacrificial hard template. This template-synthesis route is featured with a chemical "implantation" of metal ions dissolved from metalorganic compounds in nonpolar solvent to penetrate into the template surface and reside preferentially underneath the surface. Hollow particles can be easily attained by subsequent removal of the template core thermally. In comparison to the traditional hard-templating approach, advantages of such template-implantation process include: (i) the process does not require any surface modification of the template so the process is general and can extend to the formation of shell materials of different chemistries and composite compositions, (ii) tunable shell structure and particle morphology with a reduced possibility of forming agglomerates are easily attainable since that a direct particle contact during the shell-forming stage is minimized because of the inward penetration of the metal cations underneath the template surface, (iii) hollow particles of multiple compositions can be prepared in one step without the tedious LBL coating and multiple precipitation/adsorption of precursors. In this study, process variables including reaction temperature, calcination temperature, and concentration of $TiCl_4$ precursor have been systematically examined with an aim that the surface area, crystallite size, and the anatase/rutile ratio of the polycrystalline TiO_2 microcapsules prepared by the solvent-assisted template-implantation route can be tailored. Photocatalytic properties of the synthesized TiO_2 capsules against methylene blue (MB) dye in water were then examined under UV irradiations.

2. Experimental procedure

2.1. Synthesis

Titanium (IV) chloride ($TiCl_4$, 99%, Showa Chemical Co., Japan) was used as the metal precursor. Reagent-grade anhydrous heptane (99%, $CH_3(CH_2)_5CH_3$, Sigma-Aldrich, U.S.A.) was used as received without further purification as a solvent. The $TiCl_4$ of 0.05 to 0.20 g (corresponding to 26 to 105 mM, respectively) was first dissolved in the heptane solvent (10 ml) at a reaction temperature of 55 to 90 °C, before addition of 0.25 g commercial polymer beads (Micropearl SP, 3 μm in diameter, Sekisui Chemicals, Japan) as the colloidal template. The chosen reaction temperatures were all under the boiling temperature of heptane (98 °C). The solutions were continuously agitated isothermally at the reaction temperatures for 7 h under reflux, followed by repeated centrifugation (8000 revolutions per minute, Universal 320, Hettich, Germany) and washing of the template particles by mild HCl solution (10 vol%) and acetone for 5 times, respectively. The particles were dried in vacuum, and were then heated to a temperature range of 450 to 750 °C in a tube furnace (Thermolyne, Barnstead International, U.S.A.) with an isothermal holding of 2 h in flowing air atmosphere to burn out the polymeric core and form crystallized TiO_2 shell. Note that the quantitative yield of the produced hollow spheres was found proportional to the reaction temperature employed; therefore, the reaction temperature of 75 °C was deliberately chosen for subsequent experiments in comparing pore structure and photocatalysis capability of the synthesized TiO_2 spheres.

2.2. Characterization

Particle-size distribution of the hollow capsules was measured by a dynamic light-scattering technique (DLS, Nano ZS, Malvern, U.K.) from diluted suspensions. Pore structure and Brunauer–Emmett–Teller (BET) surface area of the calcined TiO_2 hollow spheres were determined from nitrogen gas sorption–desorption (ASAP 2020, Micromeritics, U.S.A.) at the boiling point of liquid nitrogen (77.4 K). Crystalline structure of the hollow spheres was observed by X-ray diffractometry (XRD, MXP-III, Mac Science, Japan) using Cu K_α radiation ($\lambda = 1.5406$ Å) at a scanning speed of $2\ min^{-1}$ from incident angles of 20° to 80°. Field-emission scanning electron microscopy (FE-SEM, JSM-6700F, JEOL, Japan) and transmission electron microscopy (TEM, JEM-2010, JEOL, Japan) were used for the examination of surface morphology and cavity structure.

2.3. Photocatalysis

Photocatalytic experiment was conducted in aqueous solutions by a UV irradiation (200 W mercury lamp) in wavelength of 365 nm with exposure durations up to 105 min. The particulate loading in solutions was held at $0.1\ g\,l^{-1}$ and the initial MB concentration was 5×10^{-6} M. All the solutions were kept in the dark for 10 min to establish an adsorption–desorption equilibrium prior the test began. Some samples were then siphoned out from the reaction solution after different exposure times and quickly centrifuged to separate the particles from the solutions. The supernatant solutions were immediately characterized by UV–vis spectrophotometry (Lambda 800, Perkin Elmer, U.S.A.) to determine the absorption change over a range of wavelengths from 200 to 900 nm. Residual MB concentration was determined from the absorption change using a 5-point calibration curve determined from known MB solutions of different concentrations.

3. Results and discussion

3.1. Effect of reaction temperature

Fig. 1 shows sintered particle morphology and cavity structure of the TiO_2 capsules prepared by the chemical

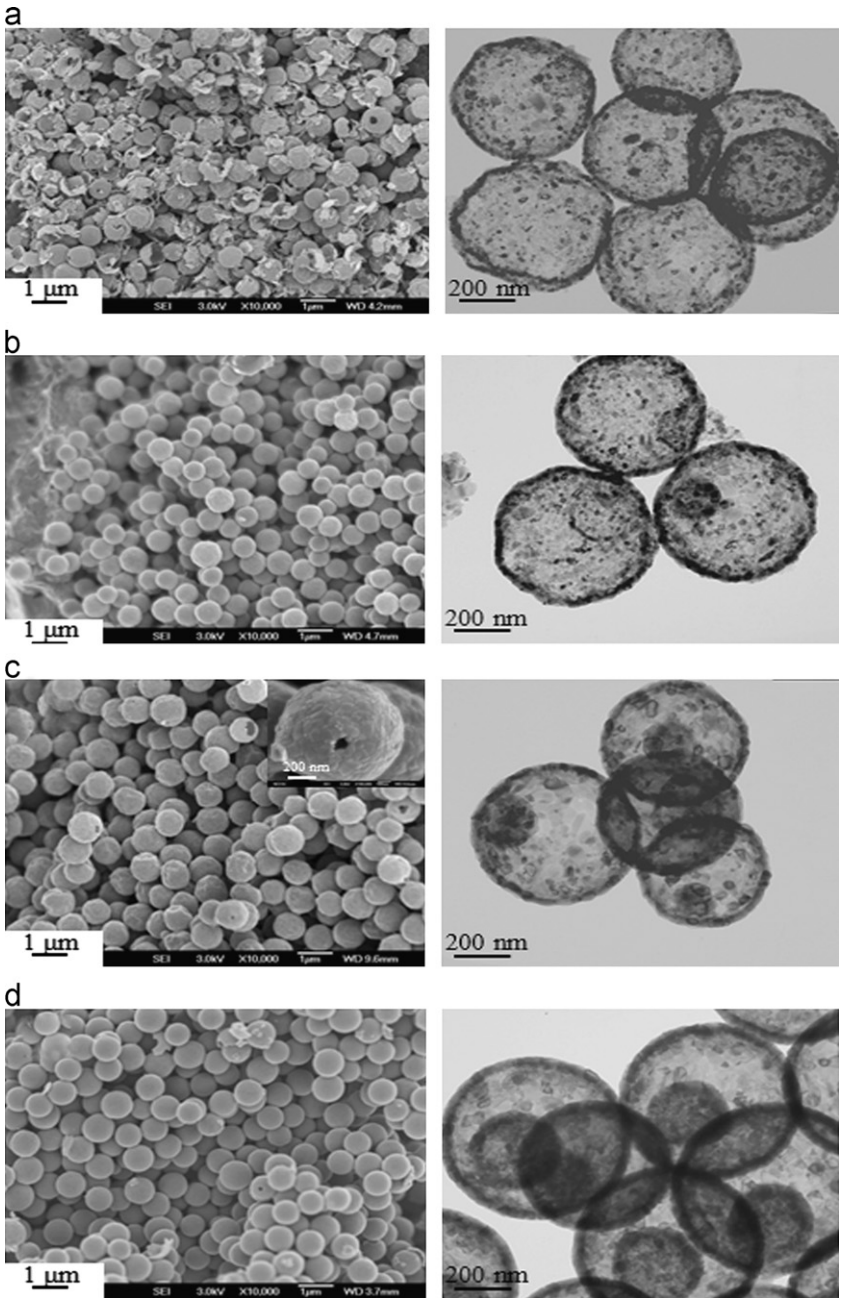

Fig. 1. Particle morphology and cavity structure of the TiO_2 hollow spheres prepared at reaction temperature of (a) 55, (b) 65, (c) 75, and (d) 90 °C. The $TiCl_4$ concentration and calcination temperature were held at 79 mM and 550 °C, respectively.

implantation method over a reaction-temperature range of 55 to 90 °C. At the reaction temperature of 55 °C, intact TiO_2 capsules were found mixing with the broken ones (Fig. 1a). As the reaction temperature was further raised, the shell thickness determined directly from the bright-field TEM images increased from ~25 nm for the sintered capsules reacted at 55 °C (Fig. 1a) to greater than ~38 nm for those reacted above 65 °C (Fig. 1b to 1d). The shell needs to become robust enough to withstand stresses involved during the capsule formation, resulted in the more intact and spherical morphology. From the TEM images, the shell is composed of assemblies of TiO_2 crystallites. No apparent necking is found between neighboring capsules. This compares favorably with the findings that the hollow spheres were indeed "flowable" in dry state, revealing that the particles were essentially agglomerate-free.

An average (sintered) particle size increases only moderately from 650 to 750 nm as the reaction temperature was increased from 55 to 90 °C. Typical standard deviation associated with the particle size measured falls in a range of ±200 nm for the capsules, revealing a broad size distribution of the prepared hollow particles. This deviation outweighs the mean size difference, so that the particle size appears relatively insensitive to the change in reaction temperatures. The sintered particle size yet shows

a pronounced dimensional shrinkage of nearly 80% when compared to that of the original template beads. Considering that the capsules would first experience a volumetric expansion during the template burnout as temperature was raised above 300 °C [24], the hollow particles were hence subjected to a substantially large compression that accompanies with the volumetric contraction when temperature was cooled down to the ambient from the calcination temperature of 550 °C. This thermally induced stress resulted in the broken spheres in Fig. 1a when the shell was too thin to bear the load.

Fig. 2 shows XRD patterns of the TiO_2 capsules prepared when the reaction temperature was varied. Both anatase (JCPDS 21-1272) and rutile (JCPDS 21-1276) phases are present in the sintered capsules. An increasing rutile intensity in conjunction with a decreasing anatase intensity is found when the reaction temperature was increased. The weight fraction of anatase (X_A) is determined from the integrated intensity of the anatase and rutile diffraction peaks by [28]

$$X_A = \frac{1}{[1+1.265(I_R/I_A)]} \tag{3.1}$$

where I_R is the integrated intensity from the rutile (1 1 0) plane, and I_A is the integrated intensity from the anatase

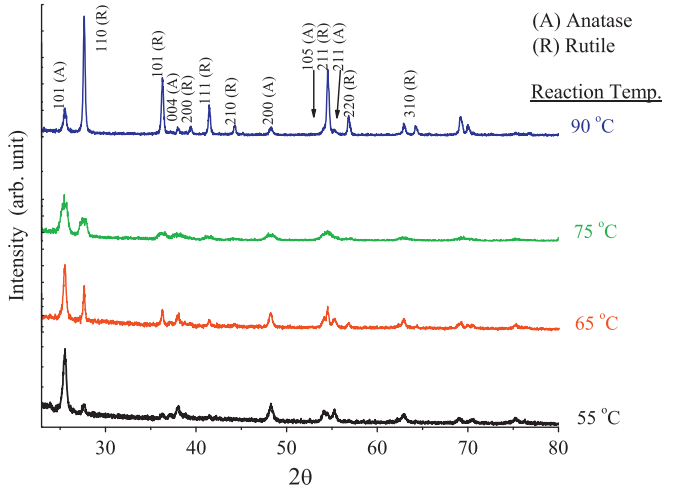

Fig. 2. X-ray diffraction patterns of the TiO_2 hollow spheres prepared at various reaction temperatures. The $TiCl_4$ concentration and calcination temperature were held at 79 mM and 550 °C, respectively.

(1 0 1) plane. In Table 1, the crystalline capsules change from a predominately anatase phase with X_A of 0.844 to a majority of rutile phase with X_A of 0.200, as the reaction temperature was increased. Exact mechanisms for the resulted anatse/rutile ratios are unclear at present. Nonetheless, Hanaor and Sorrell [29] have pointed out in a recent review that how the titanium complex joining one another critically determines the crystalline type of TiO_2 precipitated directly from chemical solutions. When the octahedra of TiO_2 complex have a sufficient energy to rearrange themselves, a linear configuration is formed with neighboring octahedra sharing two edges. This energy-favorable arrangement tends to favor the formation of rutile phase. On the contrary, the complex octahedra may form joins of zig-zag structure by sharing four edges of each octahedron upon crystallization, facilitating then formation of the anatase crystal. One might hence suspect that the reaction temperature used in the present study influences the crystallization rate of titanium precipitates in the solution and hence the crystalline phase of the shell after calcination.

The crystallite size determined by the Scherrer formula is shown in Table 1. The crystallite size remains virtually unchanged over the reaction temperatures examined for both the anatase and rutile phases. Therefore, the crystalline phase of the hollow TiO_2 spheres is critically dependent on the reaction temperature. Yet, the crystallite size is irrelevant to the reaction temperature chosen and this applies to both anatase and rutile phases.

3.2. Effect of calcination temperature

Fig. 3 shows microstructure of the TiO_2 capsules prepared at different calcination temperatures of 450, 650, and 750 °C, respectively, as the reaction temperature was kept at 75 °C. At the lower calcination temperature of 450 °C, surface of the capsules appears to be quite smooth (inset of Fig. 3a). As the calcination temperature was raised further, grain growth of the crystallites began to prevail. From the inset of Fig. 1c and Fig. 3, the shell evolves from a densely packed grain structure into an apparently porous form. In Table 2, the crystallite size is found to increase with the calcination temperature. It may be interesting to note that the calculated crystallite sizes of

Table 1
Calculated crystallite size and anatase/rutile weight percentage of the TiO_2 capsules prepared at different reaction temperatures. The $TiCl_4$ concentration and calcination temperature were held at 79 mM and 550 °C, respectively.

Reaction temp.	Crystallite size (nm)		Phase percentage (%)	
	Anatase	Rutile	Anatase	Rutile
55	20.4	102.2	84.4	15.6
65	24.1	112.8	71.0	29.0
75	23.4	100.0	66.8	33.2
90	23.4	104.7	20.0	80.0

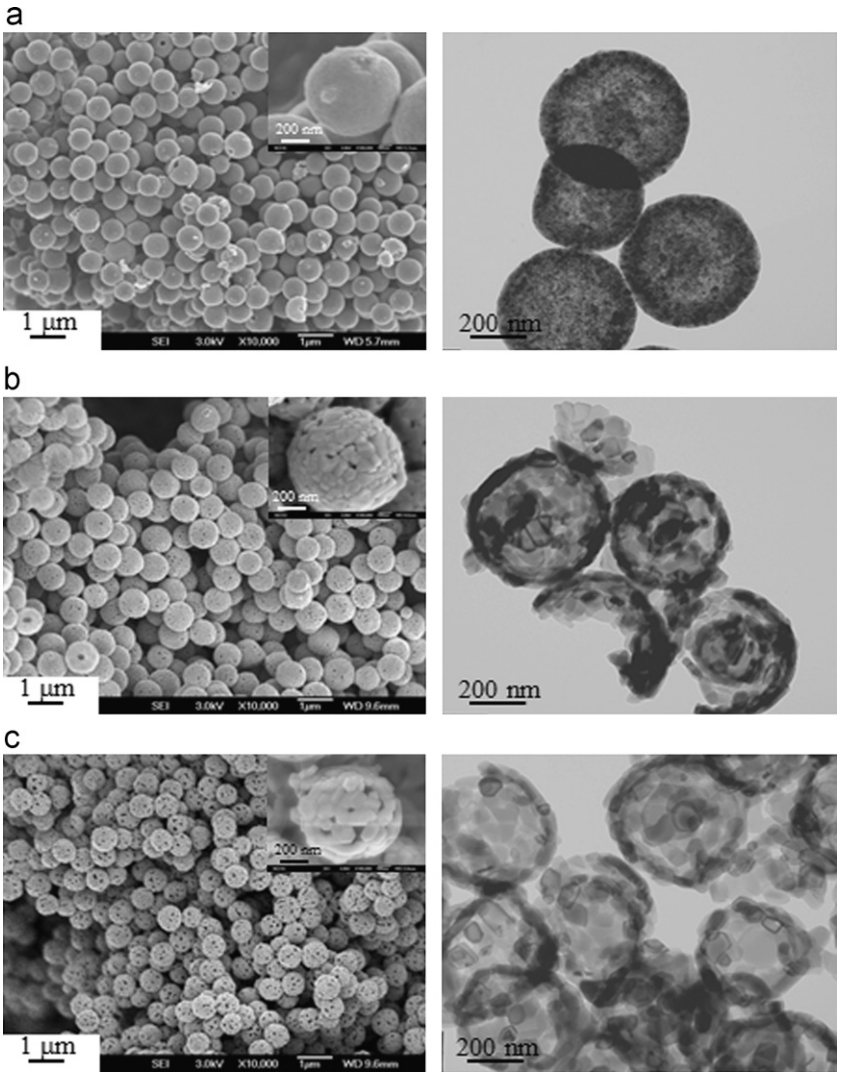

Fig. 3. Particle morphology and cavity structure of the TiO_2 hollow spheres prepared at calcination temperature of (a) 450, (b) 650, and (c) 750 °C. The $TiCl_4$ concentration and reaction temperature were held at 79 mM and 75 °C, respectively.

Table 2
Calculated crystallite size and anatase/rutile weight percentage of the TiO_2 capsules calcined at different temperatures. The $TiCl_4$ concentration and reaction temperature were held at 79 mM and 75 °C, respectively.

Calcination temp.	Crystallite size (nm)		Phase percentage (%)	
	Anatase	Rutile	Anatase	Rutile
450	16.0	82.1	93.1	6.9
550	23.4	100.0	66.8	33.2
650	N.A.	124.3	0	100.0
750	N.A.	137.1	0	100.0

N.A.: Not available.

the anatase phase are of the same order to the shell thickness observed in the TEM images, revealing that the shell may be composed of merely one anatase-structured grain in thickness, especially at the lower calcination temperature of 450 °C where the anatase structure prevailed. Coalescence of the neighboring grains proceeded upon calcination, leaving behind pores at the grain junctions (Figs. 3b and 3c) because of the thin shell involved. In Table 2, the weight fraction of anatase phase decreases accordingly from 0.931 to 0.668 as the calcination temperature was increased from 450 to 550 °C. Only the rutile phase is present when temperature was raised above

650 °C. This hence indicates that the calcination temperature critically affects the crystalline type obtained, due presumably to the anatase-to-rutile phase transformation when the grain size exceeds a certain critical size.

3.3. Effect of $TiCl_4$ concentration

Fig. 4 shows microstructure of the TiO_2 capsules prepared at different $TiCl_4$ concentrations when the reaction temperature and the calcination temperature were held at 75 and 550 °C, respectively. Broken capsules are abundant when the precursor concentration was at a low level of 26 mM in Fig. 4a, mainly due to the insufficient shell thickness to bear the compressive load when subjected to the temperature decrease upon calcination. From Fig. 1c and Fig. 4, the capsules become more intact in spherical morphology when the precursor concentration was increased, revealing that an increased shell thickness is

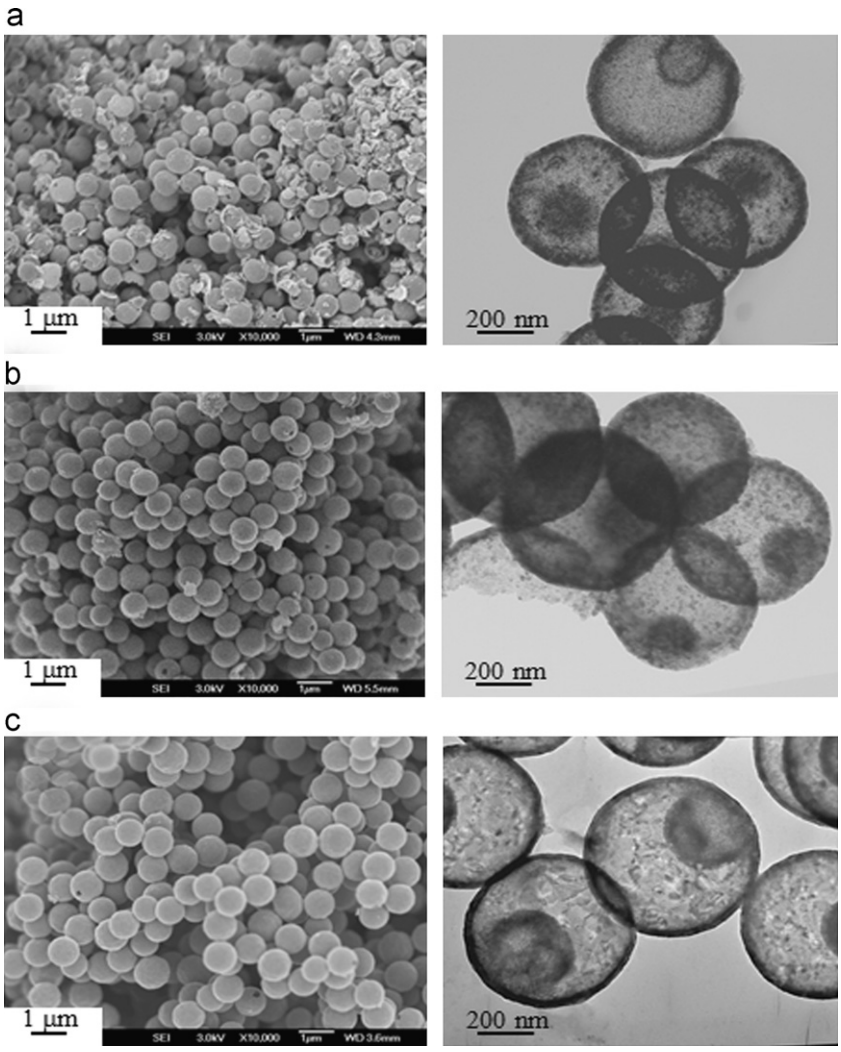

Fig. 4. Particle morphology and cavity structure of the TiO_2 hollow spheres prepared at $TiCl_4$ concentration of (a) 26, (b) 52, and (c) 105 mM. The reaction and calcination temperatures were held at 75 and 550 °C, respectively.

Table 3
Calculated crystallite size and anatase/rutile weight percentage of the TiO_2 capsules prepared at various $TiCl_4$ precursor concentrations. The reaction temperature and the calcination temperature were held at 75 and 550 °C, respectively.

$TiCl_4$ concentration	Crystallite size (nm)		Phase percentage (%)	
(mM)	Anatase	Rutile	Anatase	Rutile
26	21.6	121.8	85.5	14.5
52	19.5	128.8	83.9	16.1
79	23.4	100.0	66.8	33.2
105	22.0	113.8	77.4	22.6

formed. In Table 3, both anatase and rutile TiO_2 phases are present in the sintered capsules. The calculated crystallite size does not vary much with the precursor concentration; in addition, the anatase fraction decreases only slightly from 0.855 to 0.774 as the $TiCl_4$ concentration increased from 26 to 105 mM. This suggests that a surplus of $TiCl_4$ concentration might be used in our synthesis so that the grain size and anatase/rutile ratio of the sintered capsules were relatively insensitive to the $TiCl_4$ concentrations examined.

3.4. Pore structure of the TiO_2 capsules

Fig. 5 shows the N_2 gas sorption–desorption curves of the calcined TiO_2 capsules when the process variables were varied. As the reaction temperature increased from 55 to 90 °C, the maximum amount of N_2 gas adsorbed decreases markedly in Fig. 5a, revealing that the shell becomes denser with the increasing reaction temperature. The shells are in fact nanoporous in structure with a broad Barrett–Joyner–Halenda (BJH) pore diameter peaked at a pore diameter of ~20 nm and with a longer tail extending toward pore diameter of 100 nm. A monotonous decrease in the BET surface area (from 36.4 to 8.4 $m^2\,g^{-1}$) results when the reaction temperature was increased from 55 to 90 °C. Fig. 5b shows the N_2 sorption–desorption curves of the TiO_2 capsules calcined at various sintering temperatures. A pronounced hysteresis in the pressurization–depressurization cycle is found for the TiO_2 capsules calcined at 450 °C. This indicates that the gas molecules infiltrated into the hollow chambers were difficult to be removed under the depressurization step due to the complex pore geometry in the shell structure. As the calcination temperature was raised in order from 450 to 750 °C, the total pore volume decreases accordingly with a BET surface area reducing from 43.4 to 21.0 $m^2\,g^{-1}$. In comparison, the N_2 gas sorption–desorption curves of the calcined TiO_2 capsules are relatively insensitive to the $TiCl_4$ concentration with the curve resembles one another and the BET values are all around 30 $m^2\,g^{-1}$ over the $TiCl_4$ concentrations examined. This finding compares quite favorably with the conclusions made in Section 3.3.

3.5. Photodegradation of MB dye solutions

In Fig. 6, relative concentration (C/C_o) of the MB dye reduces notably when the aqueous suspensions consisting of the TiO_2 capsules were subjected to the UV irradiation. In Fig. 6a, the degradation rate becomes more pronounced when the reaction temperature used for the production of hollow spheres reduced from 90 to 55 °C. For the hollow particles synthesized at the reaction temperature of 55 °C, the relative dye concentration reduces to nearly complete elimination within 90 min of UV exposures, similar to that of the commercial Degussa P-25 powder of the same weight concentration. As shown in Fig. 6b, both present an almost identical degradation rate of $5.5\times10^{-2}\,min^{-1}$

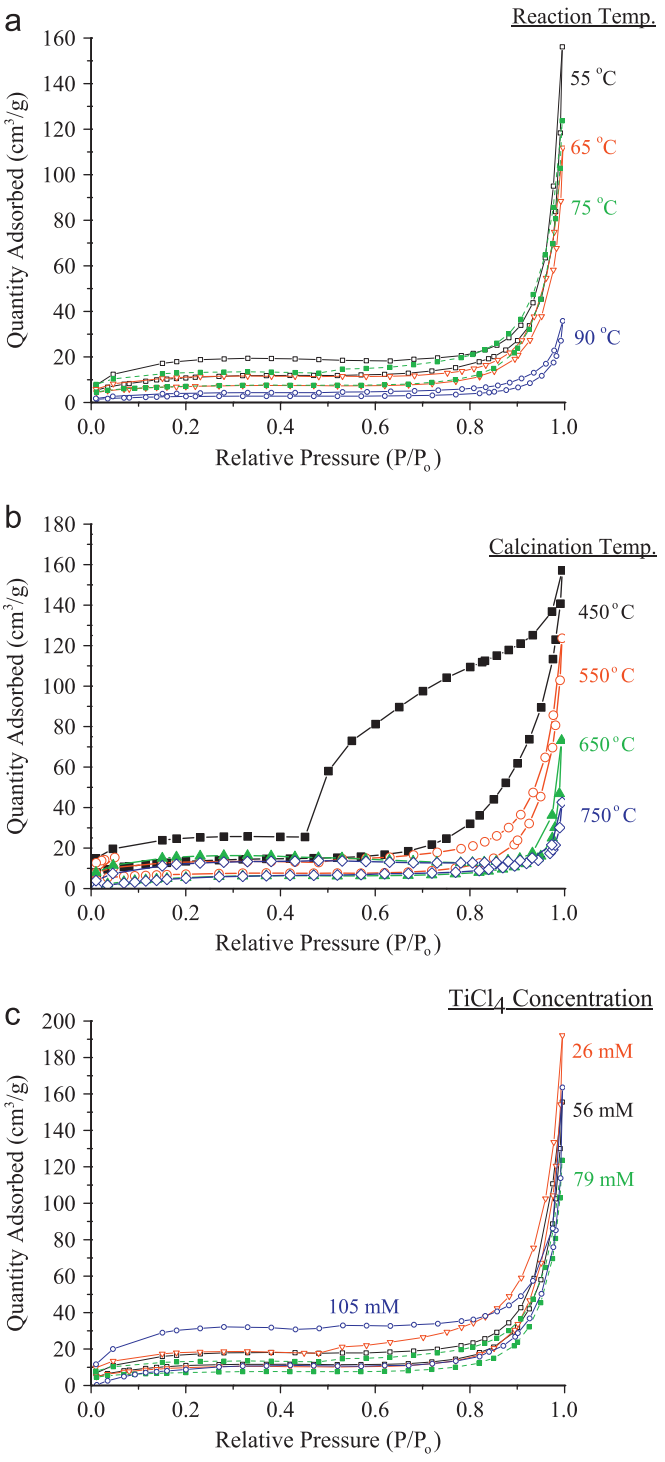

Fig. 5. Isothermal N_2 gas sorption–desorption curves of the TiO_2 hollow spheres prepared when (a) reaction temperature, (b) calcination temperature, and (c) $TiCl_4$ concentration were varied.

from the curve-fitted slopes of the logarithmic C_o/C dependence with the illumination time. This degradation rate is an order of magnitude increase from that of the TiO_2 capsules prepared at the reaction temperature of 90 °C with a degradation rate of $0.5\times10^{-2}\,min^{-1}$.

Among all the process variables examined in the study, reaction temperature used for preparing the TiO_2 hollow

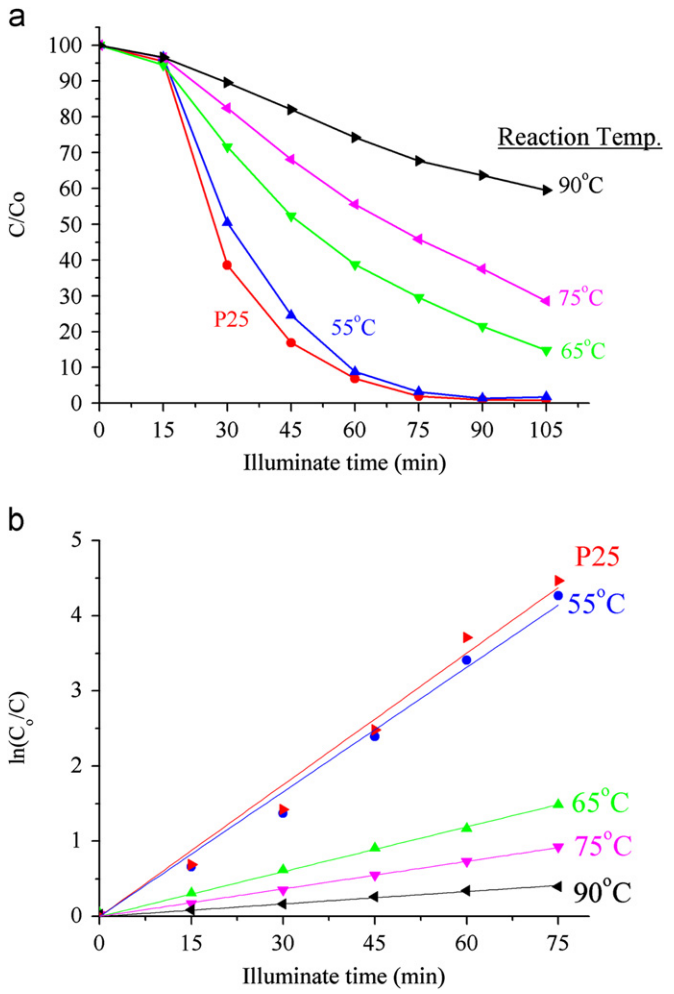

Fig. 6. (a) Photodegradation of MB dye solutions under UV irradiation. The solids concentration of the hollow TiO_2 capsules was held at 0.02 wt.% in all the suspensions. Degussa P-25 was used for comparison purposes. (b) The logarithmic concentration change with the illumination time.

spheres has been found to be the most significant parameter in determining the photocatalytic degradation of organic MB dye. For all the hollow spheres prepared by processes and material parameters other than the reaction time, none of them yields a comparable photocatalytic activity. This finding hence reveals that an increased surface area (so that an increased number of active sites for the photocatalysis to occur) together with an appropriate mixture of the anatase/rutile phases is beneficial.

4. Conclusion

Reaction temperature is the most pronounced process variables in determining the photocatalytic activity of the calcined TiO_2 microcapsules prepared by the template-implantation route. Over the reaction temperatures examined, hollow TiO_2 spheres prepared from the lowest temperature examined (55 °C) yield a photodegradation capability comparable to that of the commercial P25 powders under UV irradiations. Beside the reaction temperature, calcination temperature influences the anatase-to-rutile phase transformation and the coalescence between neighboring TiO_2 grains in the shell. A good photocatalysis can be obtained when a low calcination temperature (450 °C) is selected together with the low reaction temperature (55 °C) for the TiO_2 hollow spheres. This improved photocatalytic capability is attributable mainly to a higher BET surface area together with an appropriate anatase/rutile mixture of the hollow microcapsules.

Acknowledgment

Financial support from the National Science Council (Taiwan, R.O.C.) under contract no. NSC 98-2221-E-005-031-MY3 is gratefully acknowledged.

References

[1] M. Grätzel, Dye-sensitized solar cells, Journal of Photochemistry and Photobiology C 4 (2003) 145–153.
[2] M.R. Hoffmann, S.T. Martin, W. Choi, D.W. Bahnemann, Environmental applications of semiconductor photocatalysis, Chemical Reviews 95 (1995) 69–96.
[3] A.L. Linsebigler, G. Lu, J.T. Yates Jr., Photocatalysis on TiO_2 surfaces: principles, mechanisms, and selected properties, Chemical Reviews 95 (1995) 735–758.
[4] X. Chen, S.S. Mao, Titanium dioxide nanomaterials: synthesis, properties, modifications, and applications, Chemical Reviews 107 (2007) 2891–2959.
[5] K. Hashimoto, H. Irie, A. Fujishima, TiO_2 photocatalysis: a historical overview and future prospects, Japanese Journal of Applied Physics 44 (2005) 8269–8285.
[6] H. Li, Z. Bian, J. Zhu, D. Zhang, G. Li, Y. Huo, H. Li, Y. Lu, Mesoporous titania spheres with tunable chamber stucture and enhanced photocatalytic activity, Journal of the American Chemical Society 129 (2007) 8406–8407.
[7] D. Zhang, D. Yang, H. Zhang, C. Lu, L. Qi, Synthesis and photocatalytic properties of hollow microparticles of titania and titania/carbon composites templated by sephadex G-100, Chemistry of Materials 18 (2006) 3477–3485.
[8] D.G. Shchukin, R.A. Caruso, Template synthesis and photocatalytic properties of porous metal oxide spheres formed by nanoparticle infiltration, Chemistry of Materials 16 (2004) 2287–2292.
[9] S. Shang, X. Jiao, D. Chen, Template-free fabrication of TiO_2 hollow spheres and their photocatalytic properties, ACS Applied Materials & Interfaces 4 (2012) 860–865.
[10] Y. Kondo, H. Yoshikawa, K. Awaga, M. Murayama, T. Mori, K. Sunada, S. Bandow, S. Iijima, Preparation, photocatalytic activities, and dye-sensitized solar-cell performance of submicron-scale TiO_2 hollow spheres, Langmuir 24 (2008) 547–550.
[11] F. Caruso, X. Shi, R.A. Caruso, A. Susha, Hollow titania spheres from layered precursor deposition on sacrificial colloidal core particles, Advanced Materials 13 (2001) 740–744.
[12] L. Wang, T. Sasaki, Y. Ebina, K. Kurashima, M. Watanabe, Fabrication of controllable ultrathin hollow shells by layer-by-layer assembly of exfoliated titania nanosheets on polymer templates, Chemistry of Materials 14 (2002) 4827–4832.
[13] G.-C. Chen, C.-Y. Kuo, S.-Y. Lu, A general process for preparation of core–shell particles of complete and smooth shells, Journal of the American Ceramic Society 88 (2005) 277–283.
[14] A. Imhof, Preparation and characterization of titania-coated polystyrene spheres and hollow titania shells, Langmuir 17 (2001) 3579–3585.
[15] X. Cheng, M. Chen, L. Wu, G. Gu, Novel and facile method for the preparation of monodispersed titania hollow spheres, Langmuir 22 (2006) 3858–3863.

[16] Z.Y. Zhong, Y.D. Yin, B. Gates, Y.N. Xia, Preparation of mesoscale hollow spheres of TiO_2 and SnO_2 by templating against crystalline arrays of polystyrene beads, Advanced Materials 12 (2000) 206–209.
[17] T. Chen, P.J. Colver, S.A.F. Bon, Organic-inorganic hybrid hollow spheres prepared from TiO_2-stabilized pickering emulsion polymerization, Advanced Materials 19 (2007) 2286–2289.
[18] T.H. Eun, S.-H. Kim, W.-J. Jeong, S.-J. Jeon, S.-H. Kim, S.-M. Yang, Single-step fabrication of monodisperse TiO_2 hollow spheres with embedded nanoparticles in microfluidic devices, Chemistry of Materials 21 (2009) 201–203.
[19] A.M. Collins, C. Spickermann, S. Mann, Synthesis of titania hollow microspheres using non-aqueous emulsions, Journal of Materials Chemistry 13 (2003) 1112–1114.
[20] T. Nakashima, N. Kimizuka, Interfacial synthesis of hollow TiO_2 microspheres in ionic liquids, Journal of the American Chemical Society 125 (2003) 6386–6387.
[21] T.-Z. Ren, Z.-Y. Yuan, B.-L. Su, Surfactant-assisted preparation of hollow microspheres of mesoporous TiO_2, Chemical Physics Letters 374 (2003) 170–175.
[22] H.G. Yang, H.C. Zeng, Preparation of hollow anatase TiO_2 nanospheres via Ostwald ripening, The Journal of Physical Chemistry B 108 (2004) 3492–3495.
[23] X.W. Lou, L.A. Archer, Z. Yang, Hollow Micro-/nanostructures: synthesis and applications, Advanced Materials 20 (2008) 3987–4019.
[24] Y. Wang, W.J. Tseng, A novel technique for synthesizing nanoshell hollow alumina particles, Journal of the American Ceramic Society 92 (2009) S32–S37.
[25] T.-T. Tseng, J.Y. Uan, W.J. Tseng, Synthesis, microstructure, and photocatalysis of In_2O_3 hollow particles, Ceramics International 37 (2011) 1775–1780.
[26] W.J. Tseng, T.-T. Tseng, H.-M. Wu, Y.-C. Her, and T.-J. Yang, Facile synthesis of monodispersed In_2O_3 hollow spheres and application in photocatalysis and gas sensing, J. Am. Ceram. Soc., under review.
[27] M. Borlaf, H.-M. Wu, M.T. Colomer, R. Moreno, W.J. Tseng, Synthesis and characterization of anatase-structured titania hollow spheres doped with erbium (III), Journal of the American Ceramic Society 95 (2012) 3005–3011.
[28] R.A. Spurr, H. Myers, Quantitative analysis of anatase-rutile mixtures with an X-ray diffractometer, Analytical Chemistry 29 (1957) 760–762.
[29] D.A.H. Hanaor, C.C. Sorrell, Review of the anatase to rutile phase transformation, Journal of Materials Science 46 (2011) 855–874.